Original article

Characterization and capillary pressure curve estimation of clayey-silt sediment in gas hydrate reservoirs of the South China Sea

Yuxuan Xia[1], Sai Xu[2], Cheng Lu[3], Pål Østebø Andersen[4], Jianchao Cai[1]*

[1]*National Key Laboratory of Petroleum Resources and Engineering, China University of Petroleum, Beijing 102249, P. R. China*
[2]*School of Earth Resources, China University of Geosciences, Wuhan 430074, P. R. China*
[3]*Center of Oil & Natural Gas Resource Exploration, China Geological Survey, Beijing 100083, P. R. China*
[4]*Department of Energy Resources, University of Stavanger, 4021 Stavanger, Norway*

Abstract:
The capillary pressure curve is a crucial basis for studying the pore structure and multiphase flow characteristics in oil and gas reservoirs. Due to the loose and unconsolidated nature of the clayey-silt sediment of natural gas hydrate reservoirs in the South China Sea, conventional methods such as mercury intrusion and centrifugation struggle to obtain capillary pressure curves for these sediments. In this study, X-ray diffraction analysis, scanning electron microscopy, nitrogen adsorption, and water-gas contact angle measurements are utilized to characterize the mineral composition, pore structure, pore size distribution, and wettability of the clayey-silt sediment. Subsequently, the filter paper method from soil mechanics is employed to determine the capillary pressure curve for the clayey-silt samples. The results indicate that the capillary pressure curve obtained through the filter paper method exhibits a saturation range of 18.39%-80.31% and a capillary pressure range of 19.04 to 46,481.42 kPa. It exhibits a distinct two-stage characteristic, where capillary pressure changes rapidly with water saturation below 61.05% and slowly above 61.05%. The pore radius calculated from the capillary pressure curve ranges from 2.41 nm to 5.91 μm. This alignment with the pore ranges obtains from nitrogen adsorption and Scanning Electron Microscopy confirms the accuracy of the obtained capillary pressure curve. Furthermore, in comparison with a literature capillary pressure curve obtained through centrifugation, the paper filtration method covers a broader range, providing better representation of capillary pressure in the multiscale pores of clayey-silt samples.

1. Introduction

With the continuing rapid growth of global economy, the demand for energy resources is on the upswing. However, the exploration and development of conventional oil and gas resources has entered a bottleneck, and the difficulty of discovering new oil and gas fields is gradually increasing (Vedachalam et al., 2015; Chen et al., 2022; Bilgili, 2023). Natural gas hydrate is an important unconventional hydrocarbon resource with huge reserves worldwide, and has great potential to be a future energy source (Makogon et al., 2007;

Chong et al., 2016; Singh et al., 2022; Gajanan et al., 2024). The exploration and development of natural gas hydrate have aroused great interest in government, industry and academia (Chen et al., 2022). Owing to the improved understanding of natural gas hydrate reservoirs, many countries, including China, the United States, Japan and India, have made long-term plans and trial productions for natural gas hydrate (Boswell et al., 2012; Yamamoto et al., 2014; Li et al., 2018; Collett et al., 2019). Various methods for exploiting natural gas hydrate, including depressurization, thermal stimulation, inhibitor injection, CO_2 replacement, and mining, are in the

conceptual or field testing stages, among which the most practical and promising method for natural gas hydrate production is depressurization (Fakher et al., 2019). China has conducted two rounds of natural gas hydrate trial production in South China Sea using the depressurization method and has made great achievements (Li et al., 2018; Ye et al., 2020). However, there are still many environmental, technical and economic challenges toward future commercial production of natural gas hydrate (Zhao et al., 2017; Chibura et al., 2022; Lu et al., 2023).

The natural gas hydrate reservoir in South China Sea is unconsolidated, fine-grained clayey-silt sediment, which is quite different from the lithofacies of hydrate-bearing sediments found in other countries (Collett et al., 2012; Ito et al., 2015; Li et al., 2018). The fine-grained clayey-silt sediment containing gas hydrate is characterized by low permeability, usually less than a few millidarcy, and is therefore difficult to develop (Ye et al., 2020). In addition, the pore structure and permeability of clayey-silt sediment will change during the exploitation of gas hydrate, due to its unconsolidated structure and the decomposition of hydrate (Lu et al., 2019; Cai et al., 2020). Pore structure is crucial to the permeability and seepage characteristics of porous media. Bian et al. (2020) used computed tomography method and fractal geometry theory to probe the pore structure of clayey-silt sediment in Shenhu area, South China Sea. Qi et al. (2022) carried out CO_2 and N_2 adsorption tests on clayey-silt sediment samples acquired from the South China Sea. They found that the nanopores in clayey-silt sediments are non-uniform slit-shaped according to the hysteresis loops in N_2 adsorption-desorption isotherm. The pore structure of unconsolidated clayey-silt sediment is particularly complex, and thus further in-depth study is needed.

The capillary effect is significant in fine-grained clayey-silt sediment due to the presence of strong hydrophilic minerals and small-sized pores. Previous experimental and modeling studies have confirmed that capillary effect can greatly inhibit hydrate growth in marine sediment by reducing water activity (Clennell et al., 1999; Smith et al., 2002; Uchida et al., 2004; Liu and Flemings, 2011). During the process of gas hydrate dissociation and gas production, the capillary effect exerts a key control on the multiphase flow in marine clayey-silt sediment. The capillary pressure curve describes the capillary pressure in a porous system as a function of water saturation. Common experimental methods to obtain the capillary pressure curve of reservoir rocks include the semipermeable porous plate method, centrifuge method, and mercury injection method (Busch and Amann-Hildenbrand, 2013; Jiao et al., 2020). However, the semipermeable porous plate method is time-consuming, and the capillary pressure range measured is too small to be suitable for clayey-silt sediment with low permeability (Feng and Janssen, 2019). Similarly, the capillary pressures obtained by centrifuge are limited, reaching a few megapascals (Ruth and Wong, 1990), which is not enough to capture the complete capillary pressure curve of clayey-silt sediment (which may need tens of MPa). The most commonly used method for measuring capillary pressure, mercury injection, is time-saving and has a wide range of test pressures, but it cannot be used for clayey-silt sediment

because it is unconsolidated, and the injection of mercury will destroy the sample structure. Therefore, determining a complete and accurate capillary pressure curve of clayey-silt sediment requires specialized methods to further enable marine gas hydrate exploration and development.

Like the marine clayey-silt sediment, soil is also unconsolidated. The capillary pressure curve of soil is usually referred to as the water retention curve in the field of hydrology, where the matric suction in the water retention curve is the capillary pressure (Mahabadi et al., 2016). The water retention curve of unconsolidated porous media such as soils and clays can be measured by filter paper method. The filter paper method involves making the filter paper in close contact with the unconsolidated wet sample and sealing the whole system to prevent water evaporation. Then the filter paper wets up to a water content in equilibrium with the magnitude of the suction, and measuring of the water content of filter paper enables the determination of the matric suction from a previously established calibration curve of the filter paper used (Chandler and Gutierrez, 1986). The obtained matric suction, i.e., the capillary pressure, of filter paper is assumed to be the same as that of the sample. Although the testing time of filter paper method is relatively long, it is generally accepted to be a low-cost, reasonably accurate, and technically simple method than can be used to measure a wide range of matric suction, and has been widely applied to obtain the water retention curve of soil and clay samples (Power et al., 2008; Zhang et al., 2017; Rajesh and Khan, 2018). In this work, the filter paper method is applied for the first time to determine the capillary pressure curve of unconsolidated clayey-silt sediment in South China Sea. The capillary pressure curve is indirectly obtained by measuring the capillary pressures of the filter papers with different water content. The calculated pore sizes obtained from the capillary pressure curve are compared with those obtained from nitrogen adsorption and Scanning Electron Microscopy (SEM), and further compared with the capillary pressure curve obtained from the centrifugation method of the literature (Lei et al., 2022). These comparisons serve to validate the accuracy and effectiveness of the capillary pressure curve obtained by the filter paper method for clayey-silt sediment samples.

2. Samples and methodology

2.1 Clayey-silt samples

The region for the first offshore natural gas hydrate production test in China is located in the Baiyun sag of the Pearl River Mouth Basin in the Shenhu area, South China Sea (Li et al., 2018). The samples used in this study are directly obtained from the clayey-silt sediments in this region. The clayey-silt samples containing water appear dark gray and exhibit a state similar to that of soil. After drying, the samples appear light gray, are relatively loose, non-cemented, and are crushed into small granules (Fig. 1).

2.2 Experiments

In order to characterize the mineral composition, pore structure, and wettability of the clayey-silt sediment samples, the experimental methods employed in this study include X-

Fig. 1. Clayey-silt sediment dried samples.

Ray Diffraction analysis (XRD), SEM, low-temperature nitrogen adsorption, and contact angle measurements for wettability.

XRD involves subjecting a target to X-ray diffraction, analyzing its diffraction pattern, and obtaining information about the target's minerals. By comparing the diffraction data of the target with that of standard reference materials, the presence of specific phases in the target can be identified. Furthermore, by assessing the intensity of diffraction patterns, the content of each phase in the material can be determined. After drying and grinding the sample into powders, mineral and clay composition are tested using the BRUKER D8 ADVANCE X-ray diffractometer.

SEM employs a finely focused electron beam to scan the sample surface point by point, eliciting various electron signals with distinct functionalities. These signals are selectively collected and processed by detectors, and the resulting electron signals are transformed into images. SEM adjusts the image resolution and scanning field by manipulating the magnification. As the resolution increases and the field of view decreases, continuous adjustment of the magnification is necessary to obtain a comprehensive information of the sample. After drying the sample, it is affixed to the specimen stage with a certain length of conductive adhesive and coated with a layer of platinum to enhance electron reflectance. Observations of pore types and mineral morphologies in the sample are made at different magnifications ranging from 30 to 10,000 times.

After obtaining nitrogen adsorption-desorption isotherms under various pressures at low temperatures, based on the national standard (GB/T 19587-2004), the specific surface area of the samples is calculated using the Brunauer-Emmett-Teller equation (Brunauer et al., 1938). The Barrett-Joyner-Halenda method is employed to determine the pore volume, average pore diameter and pore size distribution of the samples (Barrett et al., 1951). The Micromeritics ASAP 2020 fully automated adsorption instrument is used to conduct low-temperature nitrogen adsorption tests on the sample. After drying, the sample is thoroughly degassed under high-temperature vacuum for 4 hours to remove impurity gases. Subsequently, it is connected to the instrument analysis system and placed in a Dewar bottle containing liquid nitrogen. Isothermal physical adsorption-desorption measurements are performed at 77.3 K in liquid nitrogen, with a relative pressure (P/P_0) range of 0.001 to 0.998.

Contact angle measurement is a direct method for assessing the wettability of a sample. The wettability angle refers to the angle formed between the tangent line of the liquid droplet interface at the three-phase boundary and the interface between the liquid droplet and the solid.

2.3 Capillary pressure curve determination using the filter paper method

To determine the capillary pressure curve of unconsolidated clayey-silt sediments, the "Double Circle" No. 203 quantitative filter papers with a diameter of 70 mm produced by Hangzhou Xinhua Paper Industry Co., Ltd. are used. The calibration curve of "Double Circle" No. 203 quantitative filter papers acquired by Wang et al. (2003) is:

$$\begin{cases} \lg S = 5.493 - 0.0767 w_f, & w_f \le 47\% \\ \lg S = 2.470 - 0.0120 w_f, & w_f > 47\% \end{cases} \quad (1)$$

where w_f represents the mass moisture content of the filter paper (%, defined as the ratio of the mass of water to the mass of sample particles), S represents capillary pressure (kPa).

When the moisture transfer between the filter paper and the sediment sample reaches equilibrium, the water saturation S_w of the sample can be expressed as:

$$S_w = \frac{w d_s}{e} \quad (2)$$

where w is the mass moisture content of the clayey-silt sediment sample, d_s represents the dimensionless relative density of the particles in the clayey-silt sediment sample, which is the ratio of the true density of the sample particles to the density of pure water ($d_s = \rho_s/\rho_w$). After measurement by G-DenPyc 2900 full automatic powder true density analyzer, the true density ρ_s of the particles is measured as 2.65 g/cm^3 according to the Boyle's law. The density of water ρ_w is taken as 1 g/cm^3. Therefore, the relative density d_s is 2.65. The symbol e denotes pore space ratio, defined as the ratio of the void volume v_v to the particle volume v_s, i.e.:

$$e = \frac{v_v}{v_s} \quad (3)$$

Eq. (3) can be transformed into the following form:

$$e = \frac{v_v}{v_s} = \frac{v - v_s}{v_s} = \frac{\dfrac{m_s}{\rho_d}}{\dfrac{m_s}{d_s \rho_w}} - 1 = \frac{d_s \rho_w}{\rho_d} - 1 \quad (4)$$

where v represents the bulk volume of the dried sample, m_s is the mass of the dried sample, and ρ_d is the bulk density of the dried sample, expressed as:

$$\rho_d = \frac{m_s}{v} \quad (5)$$

When testing the capillary pressure curve of clayey-silt samples with different moisture content using the filter paper method, the density ρ of the moist sample can be expressed as:
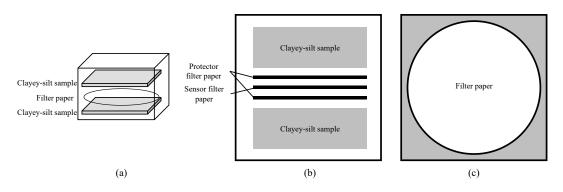
$$\rho = \frac{m}{v} \quad (6)$$

Fig. 2. Filter paper method (a) experimental schematic, (b) front view and (c) top view.

Fig. 3. Sample chamber used for filter paper method.

where m represents the mass of the wet sample.

Combing Eqs. (5) and (6) yields:

$$\rho_d = \frac{m_s \rho}{m} = \frac{\rho}{1+w} \tag{7}$$

Substituting Eq. (7) into Eq. (4) yields:

$$e = \frac{d_s \rho_w (1+w)}{\rho} - 1 \tag{8}$$

Substituting Eq. (8) into Eq. (2) gives:

$$S_w = \frac{w d_s \rho}{d_s \rho_w (1+w) - \rho} \tag{9}$$

In the implementation of the filter paper method, three filter papers were used in each set of experiments, one of which is a sensor filter paper and the other two are protector filter papers (Fig. 2). The experimental procedures of filter paper method are as follows:

1) Four small pieces of glass measuring 10 cm long and 1 cm wide are glued to a large square piece of glass measuring 11 cm side to form a sample chamber. And a total of 9 sample chambers of this size have been prepared.

2) Dry powder sediment samples with a mass of 50~60 g are placed in nine beakers, and different amounts of water were added to prepare nine samples with different moisture contents.

3) Filter papers and wet sediment samples with different moisture contents are filled into nine glass sample chambers. Make the filter papers completely embedded in the wet samples, and seal the sample chamber with vaseline

to prevent moisture evaporation (Fig. 3).

4) Filter papers and wet sediment samples are kept in full contact for 10 days to achieve a balance of moisture between them. Then open the sample chambers, take out the sensor filter paper and weigh it.

5) A small plastic container is prepared, and its mass and volume are measured as 1.7133 g and 4.0692 cm^3. The wet samples with different water saturations are used to fill the plastic container, and density of the wet samples can be calculated by weighing the mass of the wet sample in the plastic container.

6) Nine glass bottles are prepared and weighed. Fill the glass bottles with appropriate amount of samples, and the glass bottles containing the samples are placed in the oven to dry for 48 hours. Before and after drying, the mass of sensor filter papers and samples in the glass bottles are measured, and their mass moisture content can be determined.

In this experiment, the mass of dry and wet filter papers were measured and recorded. Consequently, the mass moisture content of the filter paper corresponding to 9 different test samples were determined. Combining this data with the calibration curve for the "Double Circle" No. 203 filter paper allowed the determination of the matrix suction of the samples, i.e., capillary pressure. Simultaneously, by measuring the density and mass of the samples before and after drying, the mass moisture content of the samples is determined. Then the water saturations of the samples are obtained using Eq. (9). Thus, the complete capillary pressure-saturation curve for the clayey-silt sediment sample could be determined.

3. Results and discussion

3.1 Mineral and clay composition

The sample is mainly composed of quartz (33%) and clay (32%), with additional quantities of calcite (14%), plagioclase (10%), microcline (8%), and halite (3%). Quartz content is the highest and clay content is also significant. The clay test indicates the absence of montmorillonite, with illite and illite-montmorillonite interstratification being the dominant clay minerals at 37% and 36%, respectively. Among the illite-montmorillonite interstratification, 70% is illite layers. And the sample also contains certain amounts of chlorite (16%) a-
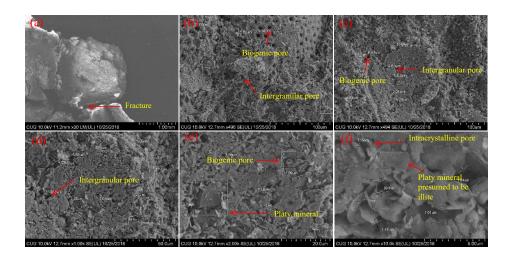
Fig. 4. SEM images at different magnifications: (a) 30x, (b) 500x, (c) 500x, (d) 1,000x, (e) 2,000x and (f) 10,000x.

Table 1. Pore and mineral properties observed through SEM.

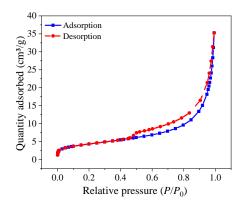| Magnification	Pore type	Pore size (μm)	Mineral	Other
30	Larger macroscopic fratures	-	-	-
500	Biogenic pores, intergranular pores	3.01-7.36	-	Regular distribution of biogenic structural pores
1,000	Biogenic pores, intergranular pores	3.09-5.90	-	Biogenic structures
2,000	Abundant biogenic pores	1.70-2.72	Platy minerals	Biogenic structures
10,000	Intracrystalline pores	0.716-1.64	Platy minerals	Presumed to be illite

Fig. 5. The nitrogen adsorption-desorption isotherm of the sample.

nd kaolinite (11%).

3.2 Pore types and mineral morphologies

The images from the SEM are shown in Fig. 4. The pores and minerals observed at different magnifications are summarized in Table 1. The predominant pore types in the sample are intergranular pores and biogenic pores, with no developed fractures. At high magnifications approaching the limit, some intracrystalline pores can be observed. The maximum pore size is 7.36 μm, and the minimum is 0.716 μm. Apart from biogenic structures, some platy minerals, presumed to be illite, are observed in the sample.

3.3 Specific surface area and pore size distribution

The nitrogen adsorption–desorption isotherm of the sample is depicted in Fig. 5. It shows a slow initial increase at relatively low relative pressures, approximately linear within a certain range. Subsequently, with further pressure increase, the isotherm departs from the linear segment and rises rapidly. Simultaneously, the adsorption isotherm and desorption isotherm in this segment do not overlap, forming a hysteresis loop. The small hysteresis loop of the sample indicates that the predominant pore shape developed in the sample is slit-like (Sing, 1985).

The specific surface area, pore volume, and average pore diameter of the sample are 15.6 m^2/g, 0.0535 cm^3/g, and 12.7 nm, respectively. Fig. 6 illustrates the pore size distribution curve of the sample. The overall curve shows a decreasing trend in proportion with increasing pore size, but there is a certain amount of pore distribution at each pore size. The peak

Table 2. Experimental data of the filter paper method.

Experiment ID	Mass moisture content of filter paper (%)	Mass moisture content of wet sample (%)	Capillary pressuret (kPa)	Water saturation (%)
1	10.86	15.01	46,481.42	18.39
2	12.15	16.83	37,119.32	19.78
3	14.15	20.02	26,175.18	23.05
4	21.1	26.71	7,754.85	32.07
5	31.46	29.93	1,264.85	42.22
6	42.21	36.59	192.82	51.49
7	72.66	41.95	39.64	61.05
8	82.86	46.03	29.9	70.16
9	99.2	53.46	19.04	80.31

Fig. 6. Pore size distribution curve of the sample.

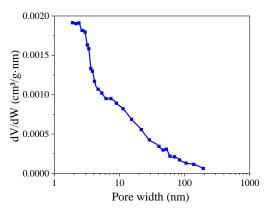**Fig. 7**. Capillary pressure curves of the clayey-silt samples.

pore diameter is mainly distributed around 2-3 nm, indicating the presence of a significant number of nanopores in the sample.

3.4 Wettability

Using the KRÜSS contact angle measuring instrument, the contact angle of the sample is measured using the captive bubble method. Prior to the test, it is necessary to prepare a cylindrical container, place the clayey-silt sediment sample into the container, and position it in a water tank. A bubble is generated using a syringe and allowed to attach to the sample surface, forming a solid-liquid-gas three-phase boundary. The contact angle is then calculated from this interface. The average contact angle of the sample, measured from both sides, is 39.4°, indicating a strong hydrophilic characteristic.

3.5 Capillary pressure curve

The specific experimental data obtained by the filter paper method is shown in Table 2. The capillary pressure on the vertical axis is plotted in logarithmic form, and the moisture saturation on the horizontal axis is plotted in linear form to obtain capillary pressure curve (Fig. 7), with a saturation range of 18.39% to 80.31% and a capillary pressure range of 19.04 to 46,481.42 kPa. The capillary pressure curve of the sample clearly exhibits a two-stage characteristic. When the water sa-
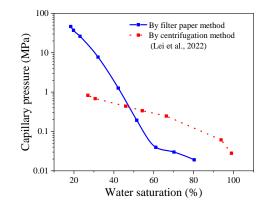
turation is less than 61.05%, the capillary pressure of the sample rapidly decreases with increasing water saturation. However, when the water saturation exceeds 61.05%, the capillary pressure decreases slowly with increasing capillary pressure.

According to the Young-Laplace equation, the pore radius r range corresponding to the capillary pressure P range obtained by the filter paper method can be calculated:

$$P = \frac{2\gamma\cos\theta}{r} \quad (10)$$

where γ is the interfacial tension between air and water, taken as 72.75 mN/m, and θ is the contact angle with a specific value measured in Section 3.4 as 39.4°. Therefore, the corresponding pore radius for the capillary pressure obtained by the filter paper method can be calculated to be approximately 2.41 nm to 5.91 μm. This explains the widespread distribution of numerous nano- and micro-scale pores in the clayey-silt sample, consistent with nanoscale pore range obtained from nitrogen adsorption and microscale pore range obtained from SEM. This also validates the accuracy of the capillary pressure curve obtained using the filter paper method.

Furthermore, a comparison is made between the capillary pressure curves of clayey-silt samples obtained using the filter paper method and those obtained using the centrifuge method (Lei et al., 2022) (Fig. 7). Due to the limitation

of the centrifuge, and excessive rotational speed may cause the unconsolidated sample to disperse, the centrifuge speed cannot be set too high. Therefore, the range of capillary pressure obtained by the centrifugation method is relatively narrow, making it challenging to characterize the wide range of pore size distribution in the clayey-silt samples. Additionally, the maximum capillary pressure corresponding to the highest centrifuge speed is only 0.82 MPa, which is insufficient to represent the capillary pressure in the nanoscale pores of the clayey-silt samples. Therefore, comparing the capillary pressure curves obtained by the centrifugation method, the filter paper method used in this study covers a wider range, providing a better representation of capillary pressure in the multiscale pores of the clayey-silt samples.

4. Conclusions

In this study, the mineral composition, pore structure, and wettability characteristics of clayey-silt sediment samples from the South China Sea are characterized through XRD analysis, SEM images, nitrogen adsorption test, and contact angle measurement. Additionally, a comprehensive capillary pressure-saturation curve for the clayey-silt sample is obtained using the filter paper method. The following conclusions are obtained:

1) The mineral composition of the sample is mainly quartz and clay, with clay being predominantly illite and mixed-layer illite-montmorillonite clay. SEM images revealed that the sample's pores are mainly intergranular and biogenic pores. The specific surface area, pore volume, and average pore diameter are 15.6 m^2/g, 0.0535 cm^3/g, and 12.7 nm, respectively. The pore size distribution curve shows a general trend of decreasing proportion with increasing pore size, with peak pore sizes mainly distributed around 2-3 nm, indicating the presence of a large number of nanopores. The contact angle of the sample is 39.4°, indicating strong hydrophilic characteristic.

2) The capillary pressure curve obtained through the filter paper method covers a saturation range of 18.39% to 80.31%, with capillary pressure ranging from 19.04 to 46,481.42 kPa. The curve exhibits a distinct two-stage characteristic, where capillary pressure changes rapidly with water saturation below 61.05% and slowly above 61.05%. Using the Young-Laplace equation combined with the measured contact angle, the calculated pore radius corresponding to this capillary pressure range is 2.41 nm to 5.91 μm. This range is consistent with the pore range obtained from nitrogen adsorption and SEM, validating the accuracy of the capillary pressure curve calculated by the filter paper method. Comparatively, the capillary pressure curve obtained by the filter paper method covers a broader range than that obtained by the centrifugation method, providing a better representation of capillary pressure in the multiscale pores of clayey-silt samples.

Conflict of interest

The authors declare no competing interest.

References

Barrett, E. P., Joyner, L. G., Halenda, P. P. The determination of pore volume and area distributions in porous substances. I. Computations from nitrogen isotherms. Journal of the American Chemical Society, 1951, 73(1): 373-380.

Bian, H., Xia, Y., Lu, C., et al. Pore structure fractal characterization and permeability simulation of natural gas hydrate reservoir based on CT images. Geofluids, 2020, 2020: 6934691.

Bilgili, L. A systematic review on the acceptance of alternative marine fuels. Renewable and Sustainable Energy Reviews, 2023, 182: 113367.

Boswell, R., Collett, T. S., Frye, M., et al. Subsurface gas hydrates in the northern Gulf of Mexico. Marine and Petroleum Geology, 2012, 34(1): 4-30.

Brunauer, S., Emmett, P. H., Teller, E. Adsorption of gases in multimolecular layers. Journal of the American Chemical Society, 1938, 60(2): 309-319.

Busch, A., Amann-Hildenbrand, A. Predicting capillarity of mudrocks. Marine and Petroleum Geology, 2013, 45: 208-223.

Cai, J., Xia, Y., Lu, C., et al. Creeping microstructure and fractal permeability model of natural gas hydrate reservoir. Marine and Petroleum Geology, 2020, 115: 104282.

Chandler, R. J. Gutierrez, C. I. The filter-paper method of suction measurement. Géotechnique, 1986, 36(2): 265-268.

Chen, X., Lu, H., Gu, L., et al. Preliminary evaluation of the economic potential of the technologies for gas hydrate exploitation. Energy, 2022, 243: 123007.

Chibura, P. E., Zhang, W., Luo, A., et al. A review on gas hydrate production feasibility for permafrost and marine hydrates. Journal of Natural Gas Science and Engineering, 2022, 100: 104441.

Chong, Z., Yang, S., Babu, P., et al. Review of natural gas hydrates as an energy resource: Prospects and challenges. Applied Energy, 2016, 162: 1633-1652.

Clennell, M. B., Hovland, M., Booth, J. S., et al. Formation of natural gas hydrates in marine sediments: 1. Conceptual model of gas hydrate growth conditioned by host sediment properties. Journal of Geophysical Research: Solid

Earth, 1999, 104(B10): 22985-23003.

Collett, T. S., Boswell, R., Waite, W. F., et al. India national gas hydrate program expedition 02 summary of scientific results: Gas hydrate systems along the eastern continental margin of India. Marine and Petroleum Geology, 2019, 108: 39-142.

Collett, T. S., Lee, M. W., Zyrianova, M. V., et al. Gulf of Mexico gas hydrate joint industry project Leg II logging-while-drilling data acquisition and analysis. Marine and Petroleum Geology, 2012, 34(1): 41-61.

Fakher, S., Elgahawy, Y., Abdelaal, H. A comprehensive review on gas hydrate reservoirs: Formation and dissociation thermodynamics and rock and fluid properties. Paper IPTC 19373 Presented at the International Petroleum Technology Conference, Beijing, China, 26-28 March, 2019.

Feng, C., Janssen, H. Hygric properties of porous building materials (IV): Semi-permeable membrane and psychrometer methods for measuring moisture storage curves. Building and Environment, 2019, 152: 39-49.

Gajanan, K., Ranjith, P. G., Yang, S. Q., et al. Advances in research and developments on natural gas hydrate extraction with gas exchange. Renewable and Sustainable Energy Reviews, 2024, 190: 114045.

Ito, T., Komatsu, Y., Fujii, T., et al. Lithological features of hydrate-bearing sediments and their relationship with gas hydrate saturation in the eastern Nankai Trough, Japan. Marine and Petroleum Geology, 2015, 66: 368-378.

Jiao, L., Andersen, P. Ø., Zhou, J., et al. Applications of mercury intrusion capillary pressure for pore structures: A review. Capillarity, 2020, 3(4): 62-74.

Lei, X., Yao, Y., Qin, X., et al. Pore structure changes induced by hydrate dissociation: An example of the unconsolidated clayey-silty hydrate bearing sediment reservoir in the South China Sea. Marine Geology, 2022, 443: 106689.

Li, J., Ye, J., Qin, X., et al. The first offshore natural gas hydrate production test in South China Sea. China Geology, 2018, 1(1): 5-16.

Liu, X., Flemings, P. B. Capillary effects on hydrate stability in marine sediments. Journal of Geophysical Research: Solid Earth, 2011, 116(B7): B07102.

Lu, C., Qin, X., Sun, J., et al. Research progress and scientific challenges in the depressurization exploitation mechanism of clayey-silt natural gas hydrates in the northern South China Sea. Advances in Geo-Energy Research, 2023, 10(1): 14-20.

Lu, C., Xia, Y., Sun, X., et al. Permeability evolution at various pressure gradients in natural gas hydrate reservoir at the Shenhu Area in the South China Sea. Energies, 2019, 12(19): 3688.

Mahabadi, N., Dai, S., Seol, Y., et al. The water retention curve and relative permeability for gas production from hydrate-bearing sediments: Pore-network model simulation. Geochemistry, Geophysics, Geosystems, 2016, 17(8): 3099-3110.

Makogon, Y. F., Holditch, S. A., Makogon, T. Y. Natural gas-hydrates-A potential energy source for the 21st Century. Journal of Petroleum Science and Engineering, 2007, 56(1): 14-31.

Power, K. C., Vanapalli, S. K., Garga, V. K. A revised contact filter paper method. Geotechnical Testing Journal, 2008, 31(6): 461-469.

Qi, R., Qin, X., Lu, C., et al. Experimental study on the isothermal adsorption of methane gas in natural gas hydrate argillaceous silt reservoir. Advances in Geo-Energy Research, 2022, 6(2): 143-156.

Rajesh, S., Khan, V. Characterization of water sorption and retention behavior of partially saturated GCLs using vapor equilibrium and filter paper methods. Applied Clay Science, 2018, 157: 177-188.

Ruth, D., Wong, S. Centrifuge capillary pressure curves. Journal of Canadian Petroleum Technology, 1990, 29(3): 67-72.

Sing, K. S. W. Reporting physisorption data for gas/solid systems with special reference to the determination of surface area and porosity (Recommendations 1984). Pure and Applied Chemistry, 1985, 57(4): 603-619.

Singh, R. P., Lall, D., Vishal, V. Prospects and challenges in unlocking natural-gas-hydrate energy in India: Recent advancements. Marine and Petroleum Geology, 2022, 135: 105397.

Smith, D. H., Wilder, J. W., Seshadri, K. Methane hydrate equilibria in silica gels with broad pore-size distributions. AIChE Journal, 2002, 48(2): 393-400.

Uchida, T., Takeya, S., Chuvilin, E. M., et al. Decomposition of methane hydrates in sand, sandstone, clays, and glass beads. Journal of Geophysical Research: Solid Earth, 2004, 109(B5): B05206.

Vedachalam, N., Srinivasalu, S., Rajendran, G., et al. Review of unconventional hydrocarbon resources in major energy consuming countries and efforts in realizing natural gas hydrates as a future source of energy. Journal of Natural Gas Science and Engineering, 2015, 26: 163-175.

Wang, Z., Yang, J., Kuang, J., et al. Application of filter paper method in field measurement of matric suction. Chinese Journal of Geotechnical Engineering, 2003, 25(4): 405-408.

Yamamoto, K., Terao, Y., Fujii, T., et al. Operational overview of the first offshore production test of methane hydrates in the Eastern Nankai Trough. Paper OTC 25243 Presented at the Offshore Technology Conference, Houston, Texas, 5-8 May, 2014.

Ye, J., Qin, X., Xie, W., et al. The second natural gas hydrate production test in the South China Sea. China Geology, 2020, 3(2): 197-209.

Zhang, X., Mavroulidou, M., Gunn, M. J. A study of the water retention curve of lime-treated London Clay. Acta Geotechnica, 2017, 12(1): 23-45.

Zhao, J., Song, Y., Lim, X., et al. Opportunities and challenges of gas hydrate policies with consideration of environmental impacts. Renewable and Sustainable Energy Reviews, 2017, 70: 875-885.